

SeisCLIP: A seismology foundation model pre-trained by multi-modal data for multi-purpose seismic feature extraction

Xu Si¹, Xinming Wu^{1*}, Hanlin Sheng¹, Jun Zhu¹ and Zefeng Li¹

¹School of Earth and Space Sciences, University of Science and Technology of China,
Hefei, China.

*To whom correspondence should be addressed:

E-mail: xinmwu@ustc.edu.cn

Abstract

Training specific deep learning models for particular tasks is common across various domains within seismology. However, this approach encounters two limitations: inadequate labeled data for certain tasks and limited generalization across regions. To address these challenges, we develop SeisCLIP, a seismology foundation model trained through contrastive learning from multi-modal data. It consists of a transformer encoder for extracting crucial features from time-frequency seismic spectrum and an MLP encoder for integrating the phase and source information of the same event. These encoders are jointly pre-trained on a vast dataset and the spectrum encoder is subsequently fine-tuned on smaller datasets for various downstream tasks. Notably, SeisCLIP’s performance surpasses that of baseline methods in event classification, localization, and focal mechanism analysis tasks, employing distinct datasets from different regions. In conclusion, SeisCLIP holds significant potential as a foundational model in the field of seismology, paving the way for innovative directions in foundation-model-based seismology research.

Introduction

In recent years, the machine-learning or deep-learning based methods has been proved efficiently in almost every subfield of seismology [Beroza et al., 2021, Mousavi and Beroza, 2022]. These methods have consistently outperformed classical approaches in a wide range of tasks, including but not limited to denoising [Zhu et al., 2019b, Wang et al., 2021b, van den Ende et al., 2021, Yang et al., 2022, Novoselov et al., 2022], earthquake detection [Ross et al., 2018b,

Yang et al., 2021, Yano et al., 2021], phase picking [Ross et al., 2018a, Mousavi et al., 2019b, Pardo et al., 2019, Wang et al., 2019, Liu et al., 2020, Bilal et al., 2022, Feng et al., 2022, Münchmeyer et al., 2022], phase association [Ross et al., 2019, McBrearty et al., 2019a,b, Yu and Wang, 2022], localization [DeVries et al., 2018, Lomax et al., 2019, Mousavi and Beroza, 2019, Zhang et al., 2020, van den Ende and Ampuero, 2020, Zhang et al., 2022, McBrearty and Beroza, 2023], event classification [Li et al., 2018, Linville et al., 2019, Ku et al., 2020, Kim et al., 2021, Bregman et al., 2021, Kong et al., 2022], focal mechanism determination [Ross et al., 2018a, Hara et al., 2019, Tian et al., 2020, Uchide, 2020, Kuang et al., 2021, Zhu et al., 2022a] and earthquake prediction [Rouet-Leduc et al., 2017, Wang et al., 2021a, Shokouhi et al., 2021, Johnson et al., 2021, Wang et al., 2022, Borate et al., 2023]. Indeed, many existing methods focus on training specific models for individual tasks. To effectively leverage the relationships between related tasks, some researchers have proposed methods to simultaneously address multiple interrelated tasks, such as earthquake detection and picking [Zhu and Beroza, 2018, Zhu et al., 2019a, Mousavi et al., 2020], earthquake monitoring [Perol et al., 2018, Zhu et al., 2022c, Si et al., 2023], localization and magnitude estimation [Münchmeyer et al., 2021].

Dealing with tasks involving large datasets, training specific models for each task can be effective to a certain extent in obtaining good performance. While there is a vast amount of data in the field of seismology overall, not every specific seismology task has sufficient data samples. The strategy of training a unique model for each task may not work well for those with only limited datasets, such as event classification and focal mechanism determination. To overcome this challenge, transfer learning has been introduced in phase picking [Chai et al., 2020, Lapins et al., 2021, Zhu et al., 2022b, Niksejel and Zhang, 2023], event classification [Titos et al., 2019, Kim et al., 2020] and earthquake peak ground motion prediction [Jozinović et al., 2022]. Although transfer learning partially mitigates the challenge of data scarcity, its applicability remains constrained to specific sub-fields of seismology. This issue is not unique in seismology field but is a common challenge across various research domains. To address this problem and enable deep learning methods to better utilize vast amounts of data, an effective way is to train a foundation model through self-supervised learning.

A foundation model is one pre-trained on broad data, typically through supervised learning, and can be adapted (e.g., fine-tuned) to a wide range of downstream tasks [Bommasani et al., 2021] with small datasets. Meanwhile, self-supervised learning involves pre-training the model on data without the need for human-labeled annotations. This approach has been successfully applied in natural language processing (e.g., BERT [Devlin et al., 2018] and GPT [Brown et al., 2020]) and computer vision (e.g., MAE [He et al., 2022]). To train a foundation model, there are two main types of self-supervised learning: generative and contrastive. The generative approach involves predicting a part of the data from the rest of the data, while the contrastive approach focuses on learning features based on discriminative signals between different data samples. CLIP [Radford et al., 2021] is one of the most popular foundation model trained by contrastive approach. Trained on multimodal data, it excels in various downstream tasks, such as image generation [Vinker et al., 2022], segmentation [Xu et al., 2022] and video classification [Luo et al., 2022]. While most of the research in this area has been focused on image and text

data, some researchers have also successfully extended these ideas to audio data, leading to the training of audio foundation models like AST [Gong et al., 2021], SSAST [Gong et al., 2022], AudioCLIP [Guzhov et al., 2022] and CAV-MAE [Gong et al., 2023].

Drawing inspiration from AudioCLIP, AST and recognizing the analogous nature of audio signals and earthquake waveforms as one-dimensional signals, we introduce SeisCLIP, a seismology foundation model pre-trained through contrastive learning on multi-modal data of seismic spectrum and event information (phase and source information). We constructed our the foundation model with a two-branch architecture of a Transformer encoder and a simple MLP for the input seismic spectrum and event information, respectively. We built the vast amount of multi-modal training data from the STEAD [Mousavi et al., 2019a] for pre-training the foundation model. In the pre-training process based on contrastive learning, by contrasting the seismic spectrum features extracted by the Transformer encoder and the seismic event information integrated by the MLP encoder, the Transformer encoder will develop the general capability of extracting crucial features that comprehensively represent the seismic data from both local and global perspectives. This general feature extraction capability acquired by the Transformer encoder through pre-training means that it can be broadly adapted to various seismic data analysis tasks. In all of our evaluation tests on the tasks event classification, location, and focal mechanism analysis associated with different datasets, the pre-trained Transformer encoder consistently outperformed traditional baseline models. This demonstrated the powerful feature extraction capability of the Transformer encoder as well as the versatility and generalizability of this capability. To better understand this capability, we visualized and compared the reduced features of the Transformer encoder with the pre-training and other training strategies. In addition, we discussed the generalization ability of SeisCLIP, considering its potential to be adapted to different datasets and tasks beyond the pre-training domain.

Methods

Architecture of the Seismology Foundation Model

Following the principles of CLIP, our goal is to develop a foundational model in seismology using contrastive learning for pre-training. The architecture of foundational models is mostly constructed with Transformer blocks [Vaswani et al., 2017], and their training is typically quite time-consuming. To improve computational efficiency, in the case of images, a common approach involves partitioning a single image (often in the size of 256×256) into smaller patches, a series of embedding operations and feeding them into the Transformer network. However, unlike 2D images, seismic waveforms are often 1D long time series, with a waveform often comprising as many as 6000 or even more samples versus an image's 256×256 dimensions. Acknowledging the limitations posed by the length of seismic waveforms, dividing signals into multiple patches can curtail the information contained within each patch. This can also disrupt the continuity of the signal, thus complicating network training. Hence, we refrained from

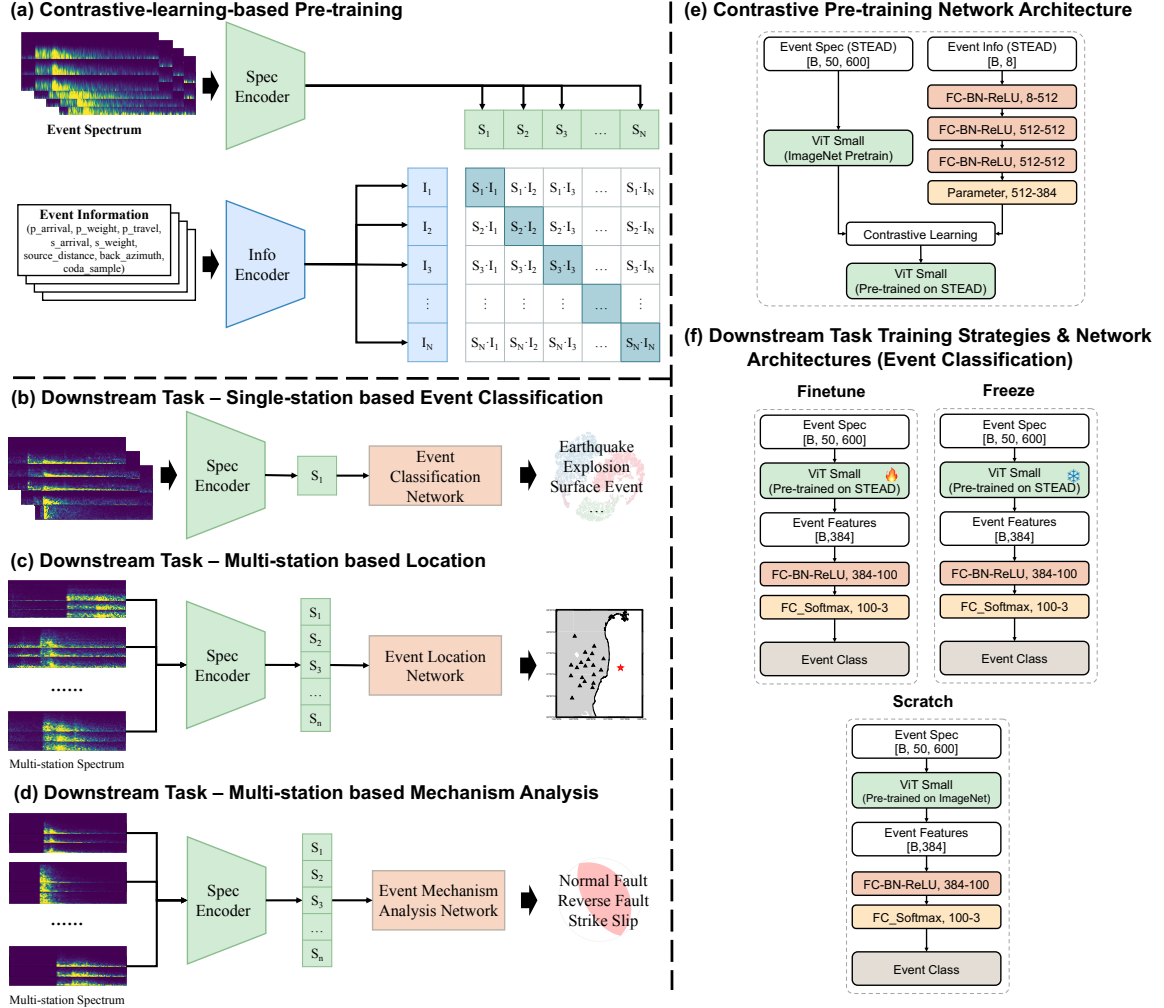


Figure 1: Summary of SeisCLIP. (a) SeisCLIP consists of two encoders that are pre-trained jointly by contrastive learning on multi-modal data of seismic spectrum and the corresponding event information (phase and source). (b - d) In downstream tasks, the pre-trained spectrum decoder is employed to generate features, which are then fed to separate sub-networks for event classification, localization, and focal mechanism analysis. (e) Detailed network architectures of the two encoders during the pre-training. (f) Three different training strategies and the corresponding network architectures of the downstream task of event classification. The detailed network architectures for the other downstream tasks are shown in Figure S2.

training a waveform-based seismology foundation model. Instead, we adopted a methodology inspired by audio processing techniques [Gong et al., 2021, 2022], to develop a spectrum-based seismology foundation model.

In our foundation model, the network architecture consists of two branches of encoders for

input spectrum images and event information (Figure S1a and Figure S1e), respectively. For the input of the spectrum branch, we converted the original seismic waveform data into time-frequency spectrum using the Short-Time Fourier Transform (STFT). This conversion allows the model to work with spectral representations of the seismic signals, enabling it to capture essential frequency-domain features and patterns. For the corresponding spectrum encoder, we utilized the ViT-small [Dosovitskiy et al., 2020], pre-trained on the ImageNet dataset, as the backbone. Conversely, the information branch incorporates eight types of event-related phase and source information included in the STEAD dataset: P arrival, P weight, P travel time, S arrival, S weight, source distance, back azimuth, and coda sample. These features were combined and formulated as a 1D vector fed into the information encoder of SeisCLIP. This information encoder is simply a Multi-Layer Perceptron (MLP) consisting of three layers, followed by a single-layer linear projection (Figure S1e). In summary, each training sample consists of two components of a three-channel spectrum data along with its corresponding eight types of event information. These components are separately fed into their respective encoders to generate the spectrum feature and information features. Subsequently, contrastive learning is employed to jointly train the two encoders by comparing the extracted spectrum and information features.

Data Preparation for Pre-training and Validation

During pre-training, SeisCLIP employs a contrastive training strategy, wherein a spectrum encoder and an information encoder are concurrently trained. To ensure the inclusiveness of the information data, we built the training dataset based on the STEAD dataset, which provides an extensive and diverse set of information related to earthquake events. In total, the STEAD dataset contains around 1,030,000 three-component signals accompanied by complete eight types of event information (phase and source). We employed approximately one million of these instances for training and reserved around 30,000 for validation.

In addition, we evaluated the performance of our pre-trained foundation model by utilizing three distinct downstream tasks: event classification, localization, and focal mechanism analysis. Accordingly, we collected four separate datasets for these tasks. For the event classification task, we employed the PNW dataset, encompassing six event types of earthquake, explosion, surface event, sonic boom, thunder and plane crash. However, to ensure balanced sample quantities for each event type, we excluded the small sample categories of plane crash, sonic boom and thunder and randomly selected 20,000 earthquake events from the total dataset. Details about event distribution and sample statistics are provided in Figure S1a and Table S1. In addition, to assess the generalization ability of the pre-trained model, we employed an earthquake-explosion dataset from the southern California seismology network (SCSN), which is a subset of the larger SCSN dataset [Zhu et al., 2022a]. Similar to the PNW dataset, the data underwent STFT processing with identical parameters. Specifics on event distribution and sample quantities for this dataset are presented in Figure S1d and Table S2.

For the localization task, we curated data from Japan (Figure S1b), encompassing $M > 2$ earthquakes that occurred between January 1, 2011, and December 31, 2011, including the

Mw 9.1 Tohoku sequence (Figure S1b). The dataset includes 12,000 events recorded by the 3-component High Sensitivity Seismograph Network (NIED Hi-net). These data were randomly divided into training, validation, and test sets with 10,000, 1,000, and 1,000 samples, respectively.

Furthermore, for the focal mechanism analysis task, we also collected data from Japan (Figure S1c), a region known for a significant number of earthquakes. The dataset comprises some $M > 3$ earthquakes occurring between 2011 and 2016, with their focal mechanisms calculated by Japan Meteorological Agency (JMA), totaling more than 2,700 events. The data were randomly divided into training, validation, and test sets (details in Table S1). To maintain consistency with the input format of the pre-trained SeisCLIP model, all waveform data in downstream tasks was cut into 60-second segments with a 100 Hz sample frequency. Spectra were derived through mean-std normalization and transformed into time-frequency representations via STFT.

Pre-training SeisCLIP by Contrastive Learning

During pre-training, two encoders of SeisCLIP are trained jointly by contrastive learning on multi-modal pairs of seismic spectrum and their corresponding event information (phase and source). To elaborate further, for a batch of N pairs, the two branches of encoders separately compute the spectrum and information embeddings from their respective inputs. The contrastive-learning-based pre-training is to maximize the cosine similarity of the spectrum and information embeddings for the N real pairs in the batch while minimize the cosine similarity for the $N^2 - N$ incorrect pairings [Radford et al., 2021]. By optimizing a symmetric cross-entropy loss over these similarity scores, we obtain the pre-trained SeisCLIP model including spectrum encoder and information encoder.

Throughout the pre-training process, the learning rate was 1e-4, with a batch size of 192. The model was trained for a total of 100 epochs. Due to the use of cross-entropy loss, the model exhibiting the most accurate classification performance on the validation set (55th epoch) was selected as the final pre-trained model. Subsequently, this model is ready to be deployed, utilizing the trained spectrum encoder for various downstream tasks.

Adapting SeisCLIP in Downstream Tasks

After pre-training, the spectrum encoder of the foundation model serves a threefold purpose in downstream tasks event classification, earthquake localization, and the analysis of seismic source focal mechanisms (Figures S1b-S1d). These tasks correspond respectively to single station classification, multi-station regression, and multi-station classification problems.

In the evaluation of downstream tasks, we employed three distinct strategies: fine-tune, frozen, and scratch. The details regarding the training strategy and network architecture for the event classification task is shown in Figure 1f. The fine-tune strategy involves activating the pre-trained spectrum encoder (ViT-small) for further training, while the frozen strategy keeps this encoder frozen during the training process. The model from scratch does not utilize

the seismology-based pre-trained model. Moreover, in addition to comparing the pre-trained models using different strategies, we also retrained some baseline models for evaluation. To ensure a fair comparison, we retrained two types of baseline models, one waveform-based and the other spectrum-based, to facilitate comparative analysis for each task. For the classification task, we utilized the earthquake and explosion classification network [Kong et al., 2022] for comparison. To accommodate the length of the spectrum data, minor adaptations were made to the network architecture.

For the localization and focal mechanism analysis tasks, we employed nearly identical baseline networks [van den Ende and Ampuero, 2020]. Architectural divergence exists solely in the activation function of the final layer: sigmoid for location and softmax for focal mechanism analysis. To validate the performance of the foundation model, the sub-networks for the location and focal mechanism tasks closely resemble the baseline models. The key distinction lies in the feature extraction from waveform/spectrum: while the baseline employs multi-layer convolutions, our sub-networks utilize the pre-trained spectrum encoder (Figure S2). To ensure fairness in comparison, all sub-networks and baselines are trained using the same training hyperparameters. Further training details can be found in the Table S3.

Results

Event Classification

For evaluation of the multi-class classification problem, typically one class is designated as the positive sample, while the other types serve as negative samples. Metrics are then calculated individually for each class (details in text S1). Following this approach, we plot the receiver operating characteristic (ROC) curves for each class for the five models (Figures 2a-2d). For all classes, the Area Under Curve (AUC) values of the fine-tune model were consistently better than those of the spectrum-based baseline model. Moreover, across all statistical results, the AUC values of the fine-tune model consistently outperformed the frozen model and the model from scratch. For a more intuitive analysis, the confusion matrix (Figure 2e-2f) provides a comprehensive view of the performance. The fine-tune model accurately classified a larger number of samples compared to the spectrum-based baseline model. Additionally, due to the pre-training process, the STEAD dataset only contains earthquake events, whereas the downstream task requires classification across three categories. As a result, the scratch model performs better than the frozen model, as it does not suffer from this discrepancy in event types.

After evaluating the downstream classification tasks in PNW dataset, we further examined the generalization capabilities of different models using an earthquake-explosion dataset from SCSN. With only two classes, AUC curves for binary classification are plotted in Figure S3. Compared to the PNW dataset, our SeisCLIP demonstrated a more pronounced advantage over baseline models. Notably, the AUC values for both fine-tuned model and model from scratch were higher than those of the baseline models. Additionally, the fine-tuned model attained the

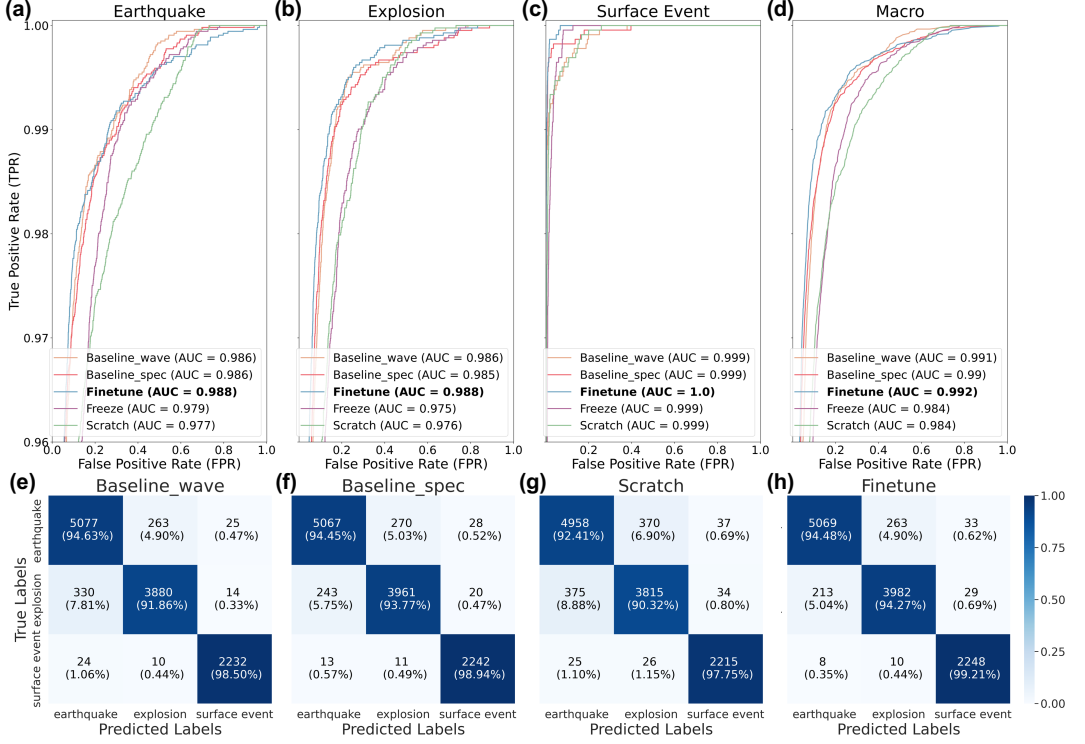


Figure 2: Evaluation metrics of different models on the event classification task. (a - c) ROC curves of five different models for the classes of earthquake, explosion, and surface event in the event classification task, respectively. In these five models, the fine-tune, scratch, and frozen models belong to SeisCLIP. (f) Macro-average represents the arithmetic mean of metrics for each class. The AUC values of each model in each class are indicated in the legend. (e - h) Confusion matrix of four models. Since the frozen model exhibited the poorest performance(the frozen model with the poorest performance is not shown here).

highest AUC value among all methods, highlighting SeisCLIP fine-tuned model’s exceptional generalization ability.

Event Location

Compared to the event classification task, our SeisCLIP method demonstrated a more significant advantage in event localization. This was evident from the residuals in epicenter distance and depth estimation, as depicted in Figure 3. In the first row of Figure 3, we displayed the epicenter distance errors associated with each event, with lighter yellow indicating smaller errors. The distribution of event points within the highlighted region (black box) of SeisCLIP (both frozen and fine-tune models) appeared shallower compared to the spectrum-based baseline (Figure 3a and 3c). This observation emphasized that the fine-tuned model exhibited lower

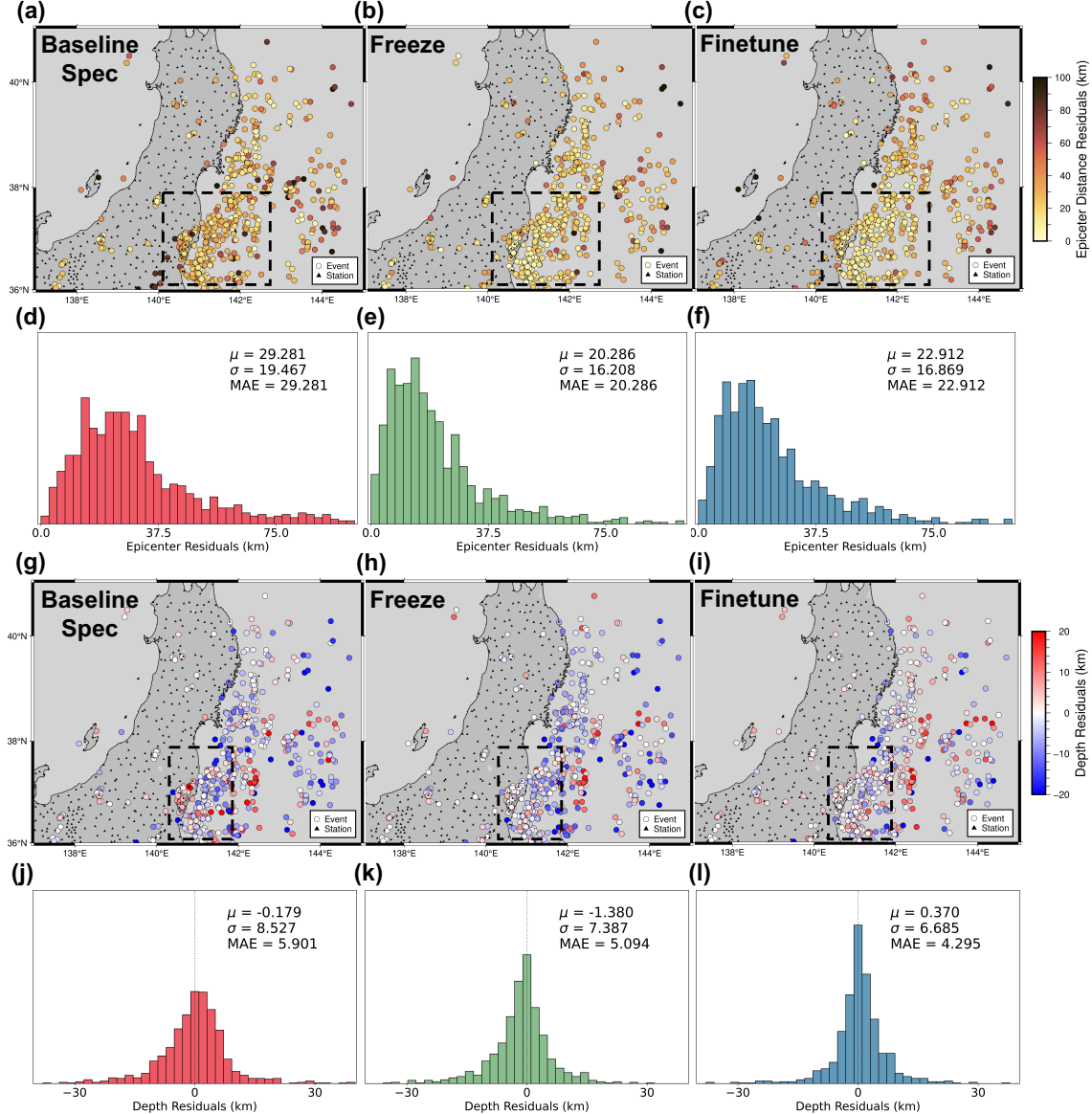


Figure 3: Performance of different models on the location task. The subfigures of a - c and g - i display the event locations of test data, where the color of dots represents the location errors. Specifically, the color in a - c corresponds to the epicenter distance residuals, while the color in g - i represents the depth residuals. The subfigures of d - f and j - l illustrate the epicenter/depth residual distributions for each model.

epicenter localization errors compared to the baseline, highlighting its distinct advantage in accurate epicenter distance estimation. Moreover, the distribution of epicenter distance errors also

supported the above observations. The error distribution of the fine-tuned model is concentrated closer to zero compared to that of the baseline methods, as seen in the second row of Figure 3 and Figure S4, indicating higher overall accuracy.

In the assessment of depth estimation, we displayed the depth errors associated with each event in the third row of Figure 3, with white denoting smaller errors. In this context, the fine-tuned model notably outperformed the frozen model and baseline model, as evident from the shallower color of event points in the highlighted region (black box) of the fine-tuned model compared to the other methods. Additionally, these findings are corroborated by the narrowest distribution of residuals and the lowest Mean Absolute Error (MAE) value in the fine-tuned model, as depicted in the fourth row of Figure 3. These results collectively underscored the superior performance of the fine-tuned model in depth estimation.

Beyond epicenter distance and depth residuals, we also analyzed the residual distributions for longitude, latitude and magnitude (depicted in Figure S4). Apart from precise position estimation, SeisCLIP also demonstrated its ability in magnitude estimation. This was evident from the narrower and more concentrated residual distribution in Figure S4, further reinforcing our pre-trained SeisCLIP method’s multifaceted advantages in event localization.

Focal Mechanism Analysis

Finally, we demonstrated the effectiveness of our foundation model for the focal mechanism analysis task. Given the challenge of determining specific focal mechanisms (strike, dip and rake) with limited training data, we opt to transform this difficult regression problem into a simpler classification problem. Here, the task is defined as a multi-station classification problem. It involves inputting multi-station features into the event mechanism analysis network, which then produces an output indicating the type of fault (normal fault, reverse fault, or strike-slip) associated with the event (Figure 1d). For this multi-class classification problem, we applied the same evaluation metrics used in the PNW dataset to assess various methods (Figure 4).

In terms of ROC curves (first row of Figure 4), SeisCLIP the best performance for all the classes of the focal mechanism analysis. Among all methods, the fine-tuned model achieved the highest AUC value, with even the frozen model significantly outperforming the spectrum-based baseline model . The confusion matrix corroborated similar results, with the fine-tuned model exhibiting the highest number of correctly classified samples, while the frozen model performed comparably well to the fine-tuned model. It’s worth noting that we have treated this task as a multi-station classification problem. Together with the previous single-station classification and multi-station regression tasks of event classification and location, we provided a comprehensive assessment of SeisCLIP’s effectiveness.

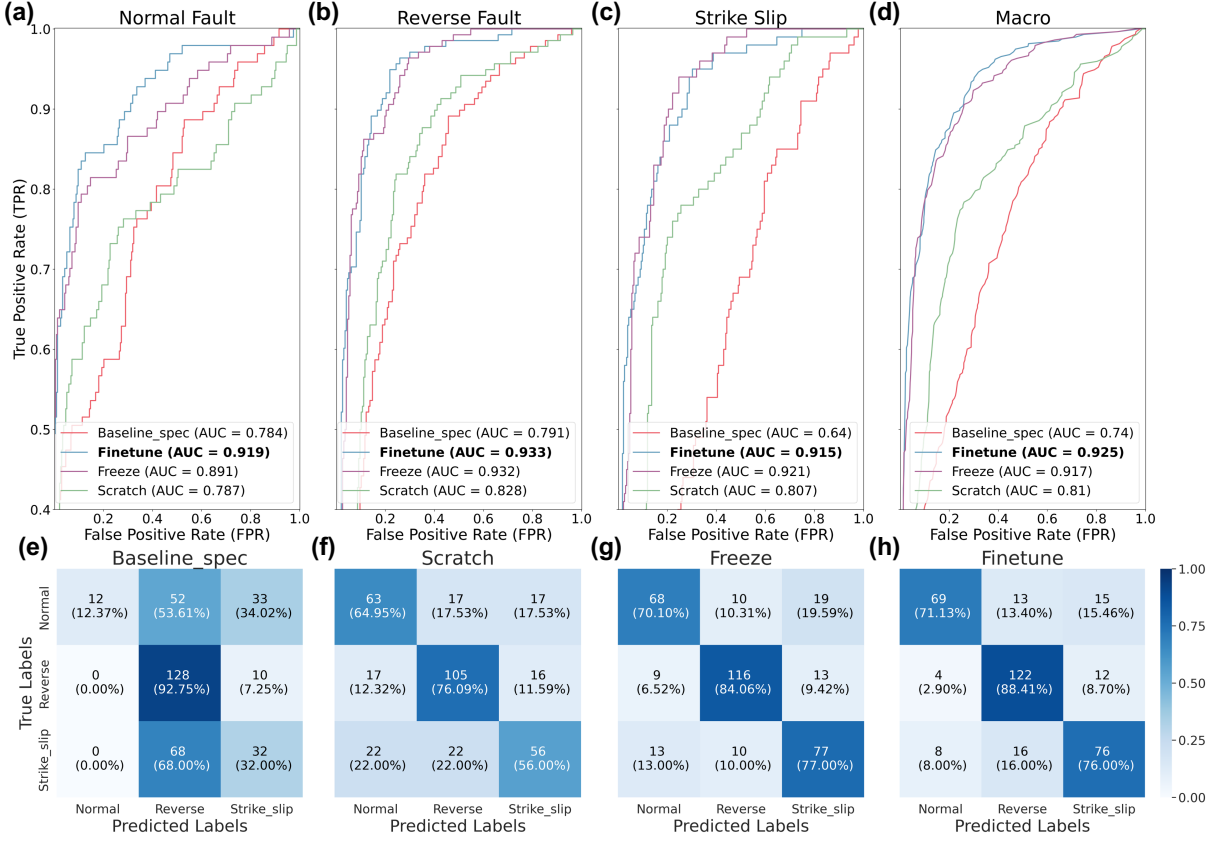


Figure 4: Evaluation metrics of four models on the task of focal mechanism analysis: (a - c) the ROC curves for each class of five different models. (d) Macro-average represents the arithmetic mean of metrics for each class. The AUC values of each model in each class are indicated in the legend. (e - h) Confusion matrix of four models.

Discussion

By initially pre-training our foundation model and subsequently fine-tuning it across various downstream tasks, SeisCLIP has demonstrated promising performance in event classification, localization, and focal mechanism analysis. To further elucidate the features captured during the pre-training process, we employed t-SNE [Van der Maaten and Hinton, 2008] to reduce the features derived from the spectrum decoder into a two-dimensional space. Subsequently, we visualized these reduced features (Figure S5) from the frozen, scratch, and fine-tuned decoders, respectively.

Since we exclusively used earthquake events to pre-train the model, the reduced features from the frozen decoder can only be identified as comcat events (comprising earthquake and explosion events) or exotic events (including surface events). Thus, we can confidently assert

Table 1: The performance of event classification and location with different spectrum size

Spec Size	Model	Event Classification			Location (MAE)		
		mPre	mRec	mF1	Epi(km)	Dep (km)	Mag($^{\circ}$)
50×120	Spec-Baseline	0.9682	0.9691	0.9687	27.97	5.57	0.51
	fine-tune (SeisCLIP)	0.9688	0.9698	0.9692	25.24	5.37	0.22
	Freeze (SeisCLIP)	0.9411	0.9443	0.9426	24.99	5.75	0.20
	Scratch (SeisCLIP)	0.9577	0.9629	0.9602	26.96	6.61	0.23
50×600	Spec-Baseline	0.9528	0.9546	0.9537	29.22	5.91	0.22
	fine-tune (SeisCLIP)	0.9557	0.9599	0.9577	22.79	4.28	0.19
	Freeze (SeisCLIP)	0.9260	0.9268	0.9263	20.27	5.10	0.22
	Scratch (SeisCLIP)	0.9334	0.9349	0.9342	29.42	6.66	0.32

Note: The metrics mprecision, mrecall, and mf1 are calculated by averaging the precision, recall, and F1-score values of the three classes. Red color represent the best performance of the spectrum size 50×120 . Blue color represent the best performance of the spectrum size 50×600 .

that our foundation model learned the intrinsic features from earthquake spectra during the pre-training. Moreover, we demonstrated that the fine-tuned model captures more substantial features compared to the model from scratch (as seen in Figure S5b and S5c) after fine-tuning. Specifically, the reduced features of explosions and surface events from the fine-tuned model were distinctly separated from the earthquake features, much more than those of the model from scratch. This visualization substantiated the efficacy of our pre-trained SeisCLIP model, emphasizing its ability to grasp essential features from earthquake spectra and its enhanced performance after fine-tuning on specific downstream tasks.

Subsequently, we analyzed the influence of different STFT parameters on the model. We set the number of frequency points to 50, spanning a frequency range from 0Hz to 50Hz. Additionally, we employed two different time samples: 120 and 600, corresponding to sampling intervals of 100 and 20, with overlaps of 50 and 10 samples, respectively, at each sampling interval. Two different foundation models were initially pre-trained using STEAD dataset, each with a different spectrum size. Then, we fine-tuned the 120-sample model and the 600-sample model using the PNW dataset and Japan location dataset respectively, employing their corresponding pre-trained models. The ensuing evaluation, utilizing identical metrics (detailed in Table 1), consistently demonstrated our model’s superiority over baseline models, regardless of the spectrum size employed. However, it’s worth noting that models pre-trained by different spectrum size were suitable for different types of tasks. In the context of classification, the distinctions in event spectra, such as those of earthquakes, explosions, and surface events, are not primarily manifested in temporal sampling. Opting for a smaller spectrum size facilitates easier model learning. On the other hand, for location, which are mainly reliant on arrival time

information, employing a larger spectrum size along the temporal dimension allows the network to achieve more precise and accurate outcomes.

The remarkable efficacy of the fine-tuned SeisCLIP model in capturing crucial features across all downstream tasks implies its potential applicability beyond the aforementioned three tasks. Theoretically, our model showcases the capability to address a diverse range of challenges similar to the aforementioned tasks, including but not limited to polarity determination, event detection, and peak ground motion estimation. However, it is crucial to acknowledge the persistent limitations within our approach. Specifically, our model may encounter challenges in generalization when different-sized spectra were applied to downstream tasks with the pre-trained model. To address this constraint and ensure the adaptability of our model across diverse subfields within seismology, we released open-source pre-trained foundation models of three distinct spectrum sizes, facilitating their customization for various downstream tasks. It is encouraged to explore other strategies to address this limitation and enhance the model's adaptability in more tasks in the future.

Conclusion

We have introduced a foundation model in seismology for event classification, location, and focal mechanism analysis. Unlike current deep learning-based methods that require training separate models for each specific task, our proposed foundation model is pre-trained on a large dataset and then fine-tuned on various tasks using smaller datasets. In doing so, our foundation model gains a comprehensive understanding of crucial features during the pre-training process but, yielding remarkable performance when adapted to various downstream tasks.

By conducting tests on multiple datasets from the different regions, our method demonstrated its capability to surpass the performance of several baseline models, achieving higher accuracy levels. The versatility showcased by our model across various downstream tasks underscores its potential to address different seismological challenges, setting a blueprint for the development of next-generation seismology deep-learning models.

Code and Data availability

The open-source foundation model can be found in <https://github.com/sixu0/SeisCLIP/>. The STEAD and PNW dataset can be downloaded from <https://github.com/smousavi05/STEAD> and <https://github.com/niyiyu/PNW-ML>. The event waveform and focal mechanism for Japan can be downloaded from HiNet (<https://www.hinet.bosai.go.jp/?LANG=en>) and the Japan Meteorological Agency (<https://www.data.jma.go.jp/svd/eqev/data/bulletin/index>).

References

- Gregory C Beroza, Margarita Segou, and S Mostafa Mousavi. Machine learning and earthquake forecasting—next steps. *Nature communications*, 12(1):4761, 2021.
- Muhammad Atif Bilal, Yanju Ji, Yongzhi Wang, Muhammad Pervez Akhter, and Muhammad Yaqub. Early earthquake detection using batch normalization graph convolutional neural network (bngcnn). *Applied Sciences*, 12(15):7548, 2022.
- Rishi Bommasani, Drew A Hudson, Ehsan Adeli, Russ Altman, Simran Arora, Sydney von Arx, Michael S Bernstein, Jeannette Bohg, Antoine Bosselut, Emma Brunskill, et al. On the opportunities and risks of foundation models. *arXiv preprint arXiv:2108.07258*, 2021.
- Prabhav Borate, Jacques Rivière, Chris Marone, Ankur Mali, Daniel Kifer, and Parisa Shokouhi. Using a physics-informed neural network and fault zone acoustic monitoring to predict lab earthquakes. *Nature Communications*, 14(1):3693, 2023.
- Y Bregman, O Lindenbaum, and N Rabin. Array based earthquakes-explosion discrimination using diffusion maps. *Pure and Applied Geophysics*, 178:2403–2418, 2021.
- Tom Brown, Benjamin Mann, Nick Ryder, Melanie Subbiah, Jared D Kaplan, Prafulla Dhariwal, Arvind Neelakantan, Pranav Shyam, Girish Sastry, Amanda Askell, et al. Language models are few-shot learners. *Advances in neural information processing systems*, 33:1877–1901, 2020.
- Chengping Chai, Monica Maceira, Hector J Santos-Villalobos, Singanallur V Venkatakrishnan, Martin Schoenball, Weiqiang Zhu, Gregory C Beroza, Clifford Thurber, and EGS Collab Team. Using a deep neural network and transfer learning to bridge scales for seismic phase picking. *Geophysical Research Letters*, 47(16):e2020GL088651, 2020.
- Jacob Devlin, Ming-Wei Chang, Kenton Lee, and Kristina Toutanova. Bert: Pre-training of deep bidirectional transformers for language understanding. *arXiv preprint arXiv:1810.04805*, 2018.
- Phoebe MR DeVries, Fernanda Viégas, Martin Wattenberg, and Brendan J Meade. Deep learning of aftershock patterns following large earthquakes. *Nature*, 560(7720):632–634, 2018.
- Alexey Dosovitskiy, Lucas Beyer, Alexander Kolesnikov, Dirk Weissenborn, Xiaohua Zhai, Thomas Unterthiner, Mostafa Dehghani, Matthias Minderer, Georg Heigold, Sylvain Gelly, et al. An image is worth 16x16 words: Transformers for image recognition at scale. *arXiv preprint arXiv:2010.11929*, 2020.
- Tian Feng, Saeed Mohanna, and Lingsen Meng. Edgephase: A deep learning model for multi-station seismic phase picking. *Geochemistry, Geophysics, Geosystems*, 23(11):e2022GC010453, 2022.

Yuan Gong, Yu-An Chung, and James Glass. Ast: Audio spectrogram transformer. [arXiv preprint arXiv:2104.01778](#), 2021.

Yuan Gong, Cheng-I Lai, Yu-An Chung, and James Glass. Ssast: Self-supervised audio spectrogram transformer. In [Proceedings of the AAAI Conference on Artificial Intelligence](#), volume 36, pages 10699–10709, 2022.

Yuan Gong, Andrew Rouditchenko, Alexander H. Liu, David Harwath, Leonid Karlinsky, Hilde Kuehne, and James R. Glass. Contrastive audio-visual masked autoencoder. In [The Eleventh International Conference on Learning Representations](#), 2023.

Andrey Guzhov, Federico Raue, Jörn Hees, and Andreas Dengel. Audioclip: Extending clip to image, text and audio. In [ICASSP 2022-2022 IEEE International Conference on Acoustics, Speech and Signal Processing \(ICASSP\)](#), pages 976–980. IEEE, 2022.

Shota Hara, Yukitoshi Fukahata, and Yoshihisa Iio. P-wave first-motion polarity determination of waveform data in western japan using deep learning. [Earth, Planets and Space](#), 71(1):1–11, 2019.

Kaiming He, Xinlei Chen, Saining Xie, Yanghao Li, Piotr Dollár, and Ross Girshick. Masked autoencoders are scalable vision learners. In [Proceedings of the IEEE/CVF conference on computer vision and pattern recognition](#), pages 16000–16009, 2022.

Paul A Johnson, Bertrand Rouet-Leduc, Laura J Pyrak-Nolte, Gregory C Beroza, Chris J Marone, Claudia Hulbert, Addison Howard, Philipp Singer, Dmitry Gordeev, Dimosthenis Karaflos, et al. Laboratory earthquake forecasting: A machine learning competition. [Proceedings of the national academy of sciences](#), 118(5):e2011362118, 2021.

Dario Jozinović, Anthony Lomax, Ivan Štajduhar, and Alberto Michelini. Transfer learning: Improving neural network based prediction of earthquake ground shaking for an area with insufficient training data. [Geophysical Journal International](#), 229(1):704–718, 2022.

Gwantae Kim, Bonhwa Ku, and Hanseok Ko. Multifeature fusion-based earthquake event classification using transfer learning. [IEEE Geoscience and Remote Sensing Letters](#), 18(6):974–978, 2020.

Gwantae Kim, Bonhwa Ku, Jae-Kwang Ahn, and Hanseok Ko. Graph convolution networks for seismic events classification using raw waveform data from multiple stations. [IEEE Geoscience and Remote Sensing Letters](#), 19:1–5, 2021.

Qingkai Kong, Ruijia Wang, William R Walter, Moira Pyle, Keith Koper, and Brandon Schmandt. Combining deep learning with physics based features in explosion-earthquake discrimination. [Geophysical Research Letters](#), 49(13):e2022GL098645, 2022.

Bonhwa Ku, Gwantae Kim, Jae-Kwang Ahn, Jimin Lee, and Hanseok Ko. Attention-based convolutional neural network for earthquake event classification. *IEEE Geoscience and Remote Sensing Letters*, 18(12):2057–2061, 2020.

Wenhuan Kuang, Congcong Yuan, and Jie Zhang. Real-time determination of earthquake focal mechanism via deep learning. *Nature communications*, 12(1):1–8, 2021.

Sacha Lapins, Berhe Goitom, J-Michael Kendall, Maximilian J Werner, Katharine V Cashman, and James OS Hammond. A little data goes a long way: Automating seismic phase arrival picking at nabro volcano with transfer learning. *Journal of Geophysical Research: Solid Earth*, 126(7):e2021JB021910, 2021.

Zefeng Li, Men-Andrin Meier, Egill Hauksson, Zhongwen Zhan, and Jennifer Andrews. Machine learning seismic wave discrimination: Application to earthquake early warning. *Geophysical Research Letters*, 45(10):4773–4779, 2018.

Lisa Linville, Kristine Pankow, and Timothy Draelos. Deep learning models augment analyst decisions for event discrimination. *Geophysical Research Letters*, 46(7):3643–3651, 2019.

Min Liu, Miao Zhang, Weiqiang Zhu, William L Ellsworth, and Hongyi Li. Rapid characterization of the july 2019 ridgecrest, california, earthquake sequence from raw seismic data using machine-learning phase picker. *Geophysical Research Letters*, 47(4):e2019GL086189, 2020.

Anthony Lomax, Alberto Michelini, and Dario Jozinović. An investigation of rapid earthquake characterization using single-station waveforms and a convolutional neural network. *Seismological Research Letters*, 90(2A):517–529, 2019.

Huaishao Luo, Lei Ji, Ming Zhong, Yang Chen, Wen Lei, Nan Duan, and Tianrui Li. Clip4clip: An empirical study of clip for end to end video clip retrieval and captioning. *Neurocomputing*, 508:293–304, 2022.

Ian W McBrearty and Gregory C Beroza. Earthquake phase association with graph neural networks. *Bulletin of the Seismological Society of America*, 113(2):524–547, 2023.

Ian W McBrearty, Andrew A Delorey, and Paul A Johnson. Pairwise association of seismic arrivals with convolutional neural networks. *Seismological Research Letters*, 90(2A):503–509, 2019a.

Ian W McBrearty, Joan Gomberg, Andrew A Delorey, and Paul A Johnson. Earthquake arrival association with backprojection and graph theoryearthquake arrival association with backprojection and graph theory. *Bulletin of the Seismological Society of America*, 109(6):2510–2531, 2019b.

S Mostafa Mousavi and Gregory C Beroza. Bayesian-deep-learning estimation of earthquake location from single-station observations. *arXiv preprint arXiv:1912.01144*, 2019.

- S Mostafa Mousavi and Gregory C Beroza. Deep-learning seismology. *Science*, 377(6607):eabm4470, 2022.
- S Mostafa Mousavi, Yixiao Sheng, Weiqiang Zhu, and Gregory C Beroza. Stanford earthquake dataset (stead): A global data set of seismic signals for ai. *IEEE Access*, 7:179464–179476, 2019a.
- S Mostafa Mousavi, Weiqiang Zhu, Yixiao Sheng, and Gregory C Beroza. Cred: A deep residual network of convolutional and recurrent units for earthquake signal detection. *Scientific reports*, 9(1):1–14, 2019b.
- S Mostafa Mousavi, William L Ellsworth, Weiqiang Zhu, Lindsay Y Chuang, and Gregory C Beroza. Earthquake transformer—an attentive deep-learning model for simultaneous earthquake detection and phase picking. *Nature communications*, 11(1):1–12, 2020.
- Jannes Münchmeyer, Dino Bindi, Ulf Leser, and Frederik Tilmann. Earthquake magnitude and location estimation from real time seismic waveforms with a transformer network. *Geophysical Journal International*, 226(2):1086–1104, 2021.
- Jannes Münchmeyer, Jack Woollam, Andreas Rietbrock, Frederik Tilmann, Dietrich Lange, Thomas Bornstein, Tobias Diehl, Carlo Giunchi, Florian Haslinger, Dario Jozinović, et al. Which picker fits my data? a quantitative evaluation of deep learning based seismic pickers. *Journal of Geophysical Research: Solid Earth*, 127(1):e2021JB023499, 2022.
- Alireza Niksejel and Miao Zhang. Obstransformer: A deep-learning seismic phase picker for obs data using automated labelling and transfer learning. *arXiv preprint arXiv:2306.04753*, 2023.
- Artemii Novoselov, Peter Balazs, and Götz Bokelmann. Sedenoss: Separating and denoising seismic signals with dual-path recurrent neural network architecture. *Journal of Geophysical Research: Solid Earth*, 127(3):e2021JB023183, 2022.
- Esteban Pardo, Carmen Garfias, and Norberto Malpica. Seismic phase picking using convolutional networks. *IEEE Transactions on Geoscience and Remote Sensing*, 57(9):7086–7092, 2019.
- Thibaut Perol, Michaël Gharbi, and Marine Denolle. Convolutional neural network for earthquake detection and location. *Science Advances*, 4(2):e1700578, 2018.
- Alec Radford, Jong Wook Kim, Chris Hallacy, Aditya Ramesh, Gabriel Goh, Sandhini Agarwal, Girish Sastry, Amanda Askell, Pamela Mishkin, Jack Clark, et al. Learning transferable visual models from natural language supervision. In *International conference on machine learning*, pages 8748–8763. PMLR, 2021.

Zachary E Ross, Men-Andrin Meier, and Egill Hauksson. P wave arrival picking and first-motion polarity determination with deep learning. *Journal of Geophysical Research: Solid Earth*, 123(6):5120–5129, 2018a.

Zachary E Ross, Men-Andrin Meier, Egill Hauksson, and Thomas H Heaton. Generalized seismic phase detection with deep learning short note. *Bulletin of the Seismological Society of America*, 108(5A):2894–2901, 2018b.

Zachary E Ross, Yisong Yue, Men-Andrin Meier, Egill Hauksson, and Thomas H Heaton. Phaselink: A deep learning approach to seismic phase association. *Journal of Geophysical Research: Solid Earth*, 124(1):856–869, 2019.

Bertrand Rouet-Leduc, Claudia Hulbert, Nicholas Lubbers, Kipton Barros, Colin J Humphreys, and Paul A Johnson. Machine learning predicts laboratory earthquakes. *Geophysical Research Letters*, 44(18):9276–9282, 2017.

Parisa Shokouhi, Vrushali Girkar, Jacques Rivière, Srisharan Shreedharan, Chris Marone, C Lee Giles, and Daniel Kifer. Deep learning can predict laboratory quakes from active source seismic data. *Geophysical Research Letters*, 48(12):e2021GL093187, 2021.

Xu Si, Ximeng Wu, Zefeng Li, Shenghou Wang, and Jun Zhu. Multi-task multi-station earthquake monitoring: An all-in-one seismic phase picking, location, and association network (plan). *arXiv preprint arXiv:2306.13918*, 2023.

Xiao Tian, Wei Zhang, Xiong Zhang, Jie Zhang, Qingshan Zhang, Xiangteng Wang, and Quanshi Guo. Comparison of single-trace and multiple-trace polarity determination for surface microseismic data using deep learning. *Seismological Research Letters*, 91(3):1794–1803, 2020.

Manuel Titos, Angel Bueno, Luz García, Carmen Benítez, and José C Segura. Classification of isolated volcano-seismic events based on inductive transfer learning. *IEEE Geoscience and Remote Sensing Letters*, 17(5):869–873, 2019.

Takahiko Uchide. Focal mechanisms of small earthquakes beneath the Japanese islands based on first-motion polarities picked using deep learning. *Geophysical Journal International*, 223 (3):1658–1671, 2020.

Martijn van den Ende, Itzhak Lior, Jean-Paul Ampuero, Anthony Sladen, André Ferrari, and Cédric Richard. A self-supervised deep learning approach for blind denoising and waveform coherence enhancement in distributed acoustic sensing data. *IEEE Transactions on Neural Networks and Learning Systems*, 2021.

Martijn PA van den Ende and J-P Ampuero. Automated seismic source characterization using deep graph neural networks. *Geophysical Research Letters*, 47(17):e2020GL088690, 2020.

Laurens Van der Maaten and Geoffrey Hinton. Visualizing data using t-sne. *Journal of machine learning research*, 9(11), 2008.

Ashish Vaswani, Noam Shazeer, Niki Parmar, Jakob Uszkoreit, Llion Jones, Aidan N Gomez, Łukasz Kaiser, and Illia Polosukhin. Attention is all you need. *Advances in neural information processing systems*, 30, 2017.

Yael Vinker, Ehsan Pajouheshgar, Jessica Y Bo, Roman Christian Bachmann, Amit Haim Bermano, Daniel Cohen-Or, Amir Zamir, and Ariel Shamir. Clipasso: Semantically-aware object sketching. *ACM Transactions on Graphics (TOG)*, 41(4):1–11, 2022.

Jian Wang, Zhuowei Xiao, Chang Liu, Dapeng Zhao, and Zhenxing Yao. Deep learning for picking seismic arrival times. *Journal of Geophysical Research: Solid Earth*, 124(7):6612–6624, 2019.

Kun Wang, Christopher W Johnson, Kane C Bennett, and Paul A Johnson. Predicting fault slip via transfer learning. *Nature Communications*, 12(1):7319, 2021a.

Kun Wang, Christopher W Johnson, Kane C Bennett, and Paul A Johnson. Predicting future laboratory fault friction through deep learning transformer models. *Geophysical Research Letters*, 49(19):e2022GL098233, 2022.

Tiantong Wang, Daniel Trugman, and Youzuo Lin. Seismogen: Seismic waveform synthesis using gan with application to seismic data augmentation. *Journal of Geophysical Research: Solid Earth*, 126(4):e2020JB020077, 2021b.

Jiarui Xu, Shalini De Mello, Sifei Liu, Wonmin Byeon, Thomas Breuel, Jan Kautz, and Xiaolong Wang. Groupvit: Semantic segmentation emerges from text supervision. In *Proceedings of the IEEE/CVF Conference on Computer Vision and Pattern Recognition*, pages 18134–18144, 2022.

Lei Yang, Xin Liu, Weiqiang Zhu, Liang Zhao, and Gregory C Beroza. Toward improved urban earthquake monitoring through deep-learning-based noise suppression. *Science advances*, 8(15):eabl3564, 2022.

Shaobo Yang, Jing Hu, Haijiang Zhang, and Guiquan Liu. Simultaneous earthquake detection on multiple stations via a convolutional neural network. *Seismological Research Letters*, 92(1):246–260, 2021.

Keisuke Yano, Takahiro Shiina, Sumito Kurata, Aitaro Kato, Fumiyasu Komaki, Shin’ichi Sakai, and Naoshi Hirata. Graph-partitioning based convolutional neural network for earthquake detection using a seismic array. *Journal of Geophysical Research: Solid Earth*, 126(5):e2020JB020269, 2021.

Ziye Yu and Weitao Wang. Fastlink: a machine learning and gpu-based fast phase association method and its application to yangbi m s 6.4 aftershock sequences. Geophysical Journal International, 230(1):673–683, 2022.

Xiong Zhang, Jie Zhang, Congcong Yuan, Sen Liu, Zhibo Chen, and Weiping Li. Locating induced earthquakes with a network of seismic stations in oklahoma via a deep learning method. Scientific reports, 10(1):1–12, 2020.

Xitong Zhang, Will Reichard-Flynn, Miao Zhang, Matthew Hirn, and Youzuo Lin. Spatio-temporal graph convolutional networks for earthquake source characterization. Journal of Geophysical Research: Solid Earth, page e2022JB024401, 2022.

Zhu, Lihua Fang, Fajun Miao, Liping Fan, Ji Zhang, and Zefeng Li. Deep learning and transfer learning of earthquake and quarry-blast discrimination: Applications to southern california and eastern kentucky. Authorea Preprints, 2022a.

Jun Zhu, Zefeng Li, and Lihua Fang. Ustc-pickers: a unified set of seismic phase pickers transfer learned for china. Earthquake Science, 36:1–11, 2022b.

Lijun Zhu, Zhigang Peng, James McClellan, Chenyu Li, Dongdong Yao, Zefeng Li, and Lihua Fang. Deep learning for seismic phase detection and picking in the aftershock zone of 2008 mw7. 9 wenchuan earthquake. Physics of the Earth and Planetary Interiors, 293:106261, 2019a.

Weiqiang Zhu and Gregory C Beroza. Phasenet: a deep-neural-network-based seismic arrival-time picking method. Geophysical Journal International, 216(1):261–273, 10 2018.

Weiqiang Zhu, S Mostafa Mousavi, and Gregory C Beroza. Seismic signal denoising and decomposition using deep neural networks. IEEE Transactions on Geoscience and Remote Sensing, 57(11):9476–9488, 2019b.

Weiqiang Zhu, Kai Sheng Tai, S Mostafa Mousavi, Peter Bailis, and Gregory C Beroza. An end-to-end earthquake detection method for joint phase picking and association using deep learning. Journal of Geophysical Research: Solid Earth, 127(3):e2021JB023283, 2022c.

Supplementary Information

Text S1. Evaluation matrix

To evaluate the classification performance of our models, we employed Receiver Operating Characteristic curves (ROC) and Area Under the Curve (AUC). For the two-class classification problem (Figure S3), the model outputs probabilities for each class (earthquake or explosion).

By applying a threshold, events in the test dataset are classified as earthquake or explosion. Therefore, we calculated True Positive (TP, correctly classified explosions), True Negative (TN, correctly classified earthquakes), False Positive (FP, earthquakes classified as explosions), and False Negative (FN, explosions classified as earthquakes) elements to derive metrics such as precision, recall, True Positive Rate (TPR), False Positive Rate (FPR), and f1-score:

$$Precision = \frac{TP}{TP + FP} \quad (1)$$

$$TPR = Recall = \frac{TP}{TP + FN} \quad (2)$$

$$FPR = \frac{FP}{FP + TN} \quad (3)$$

$$f1 = 2 \times \frac{precision \times recall}{precision + recall} \quad (4)$$

By varying the threshold and calculating TPR and FPR at each point, we obtained the ROC curve for the binary classification problem (Figure S3). The AUC value represents the overall performance of the classifier across different thresholds and ranges between 0 and 1, where higher values indicate better performance.

For multi-class classification tasks, we converted them into multiple binary classification problems using the one-vs-rest approach. For instance, to generate Figure 2, we respectively treated earthquake, explosion and surface event as positive samples, and the other two categories as negative samples to calculate TP, TN, FP, and FN for each class. This allowed us to obtain ROC curves for each class in the multi-class classification problem. Additionally, we calculated the Macro-average, representing the arithmetic mean of the metrics across multiple classes.

Text S2. Training details

During the training process, the model was optimized using the ADAM method. For different training procedures, we employed different loss function, learning rate, epochs and batch size (Table S3). All the model was selected based on the best performance on validation dataset.

Table S1: Data division of event classification and mechanism analyze tasks.

Task	Type	Train	Validation	Test	Total
Event Classification	Earthquake	13170	1350	5480	20000
	Explosion	10597	1030	4316	15943
	Surface Event	6000	598	2314	8912
Mechanism	Normal Fault	654	54	97	805
	Reverse Fault	941	88	138	1167
	Strike Slip	705	58	100	863

Table S2: Data division of event classification task for testing model's generalization ability.

Type	Earthquake	Blast
Number of Events	913	464
Number of Waveforms	18642	10435

Table S3: Training details in pre-training process and three downstream tasks.

Type	Pre-train	Classification	Location	Focal Mechanism
Learning rate	1e-4	1e-4	2e-4	1e-4
Batch Size	192	128	16	4
Epochs	100	100	200	200
Loss function	Cross-entropy	Cross-entropy	MSE	Cross-entropy

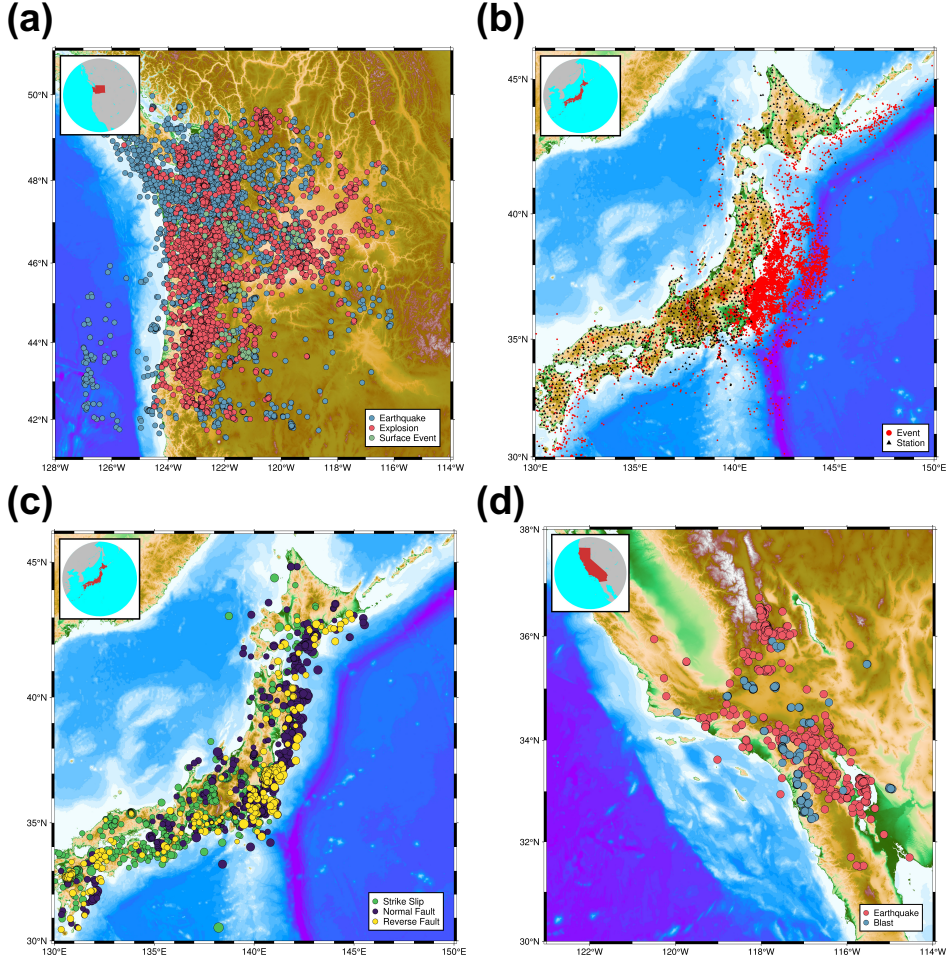


Figure S1: Spatial distributions of events for different tasks. (a) Distribution of the events used for classification task from PNW datasets. The earthquake, explosion, and surface events are colored by blue, red, and green, respectively. (b) Distribution of stations (black triangles) and event locations (red circles) used for the location task in our study, where the events occurred between January 1, 2011 and December 31, 2011. (c) Distribution of event locations used for the task of focal mechanism analysis in our study, where the green, dark blue and yellow circles respectively represent strike slip, normal fault and reverse fault. All the events occurred between 2011 and 2015. (b) Distribution of earthquakes (red circles) and explosions (blue circle) in southern California, used to test the generalization ability of the models.

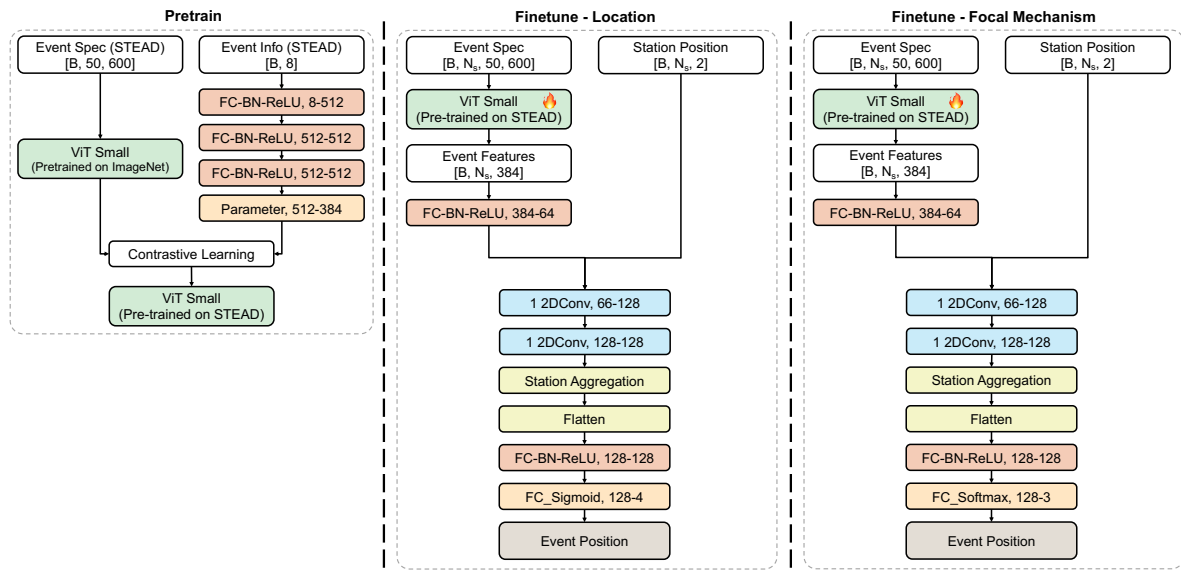


Figure S2: While using the same pre-trained spectrum decoder (left panel) as in the event classification task (Figure 1), we designed different decoder networks for the location (middle panel) and focal mechanism (right panel) tasks.

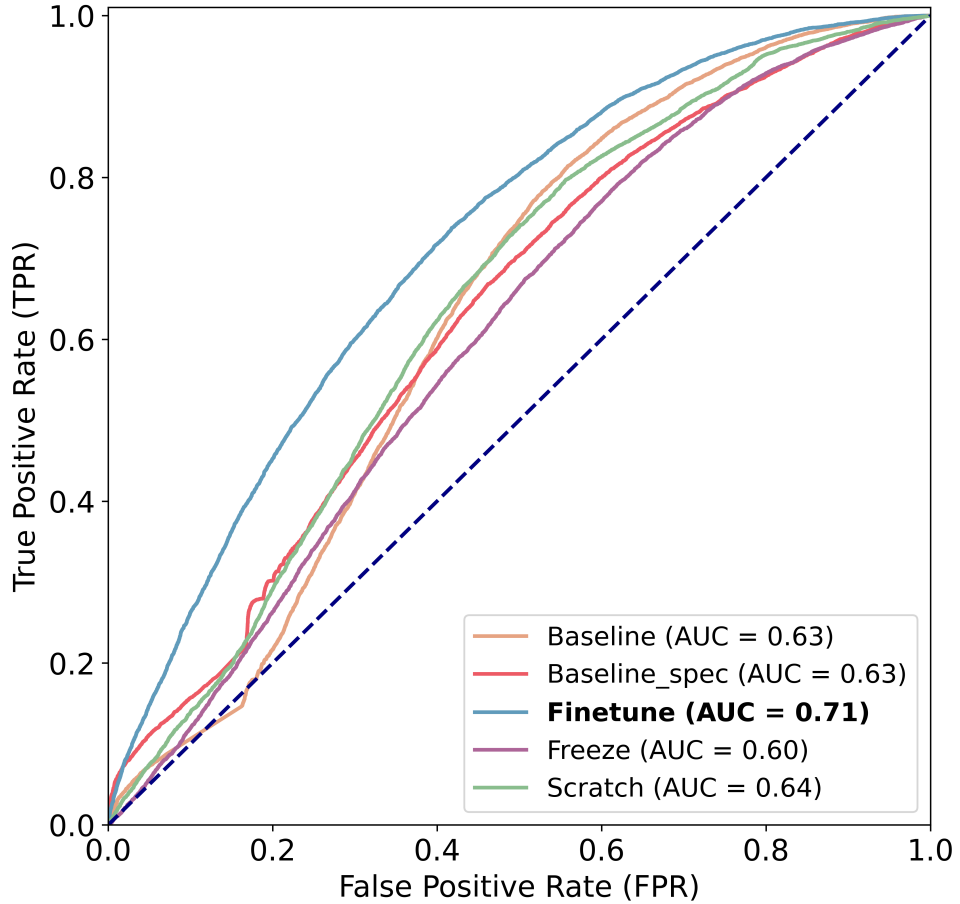


Figure S3: The ROC curves of earthquake-explosion classification task for testing models' generalization ability. All of the models are initially trained on the PNW dataset and subsequently applied to the SCSN dataset. Given that it's a binary classification problem, we can generate the ROC curve for the earthquake-explosion classification task by adjusting the threshold and calculating the True Positive Rate (TPR) and False Positive Rate (FPR) at each threshold point.

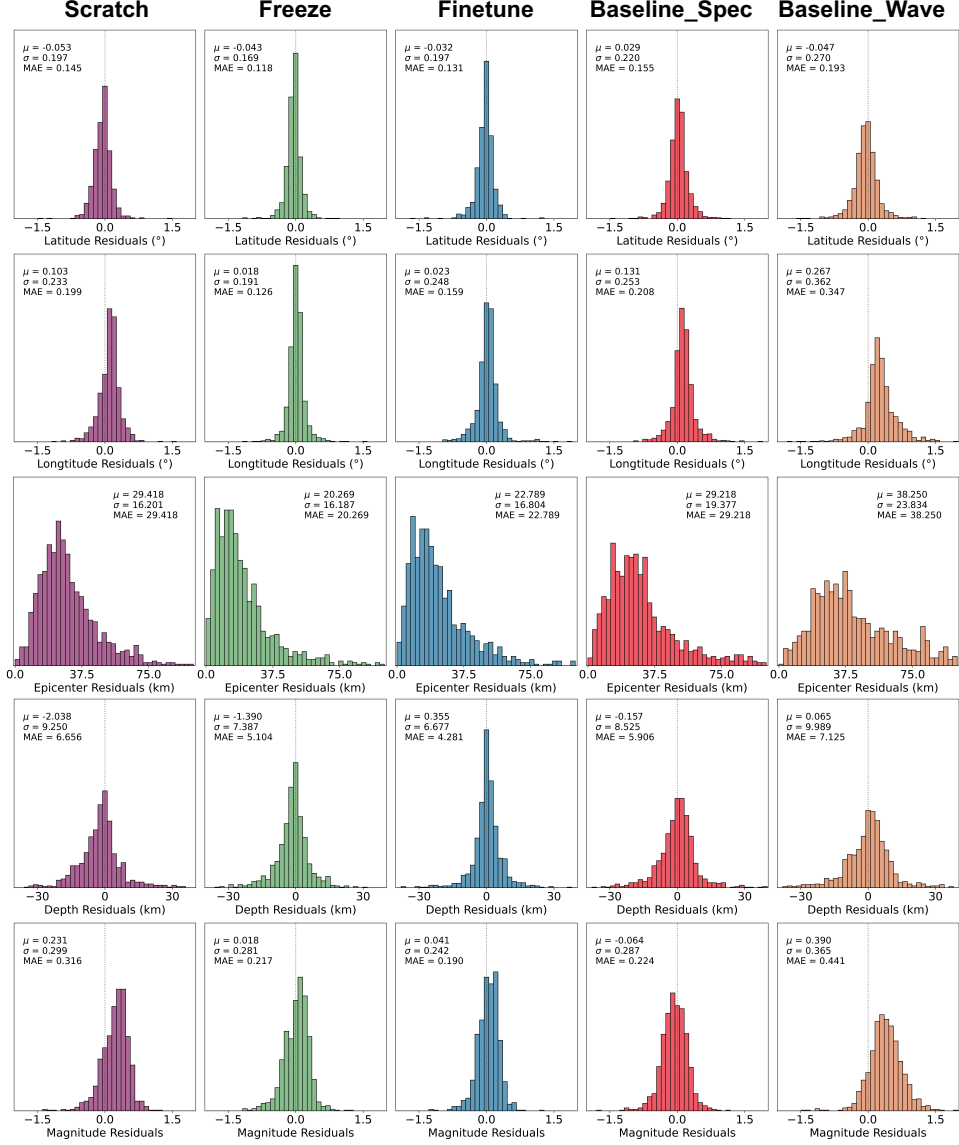


Figure S4: Distributions of residuals in localization task. The first and second rows display latitude and longitude residuals, respectively. The third row shows epicenter residuals, calculated from latitude and longitude residuals. Notably, the frozen model and fine-tuned model exhibited the best performance. Additionally, the fourth and fifth rows illustrate depth and magnitude residuals, respectively. For depth and magnitude estimation, the fine-tune model demonstrated outstanding performance, as indicated by the narrowest distribution of residuals and the lowest mean absolute error (MAE).

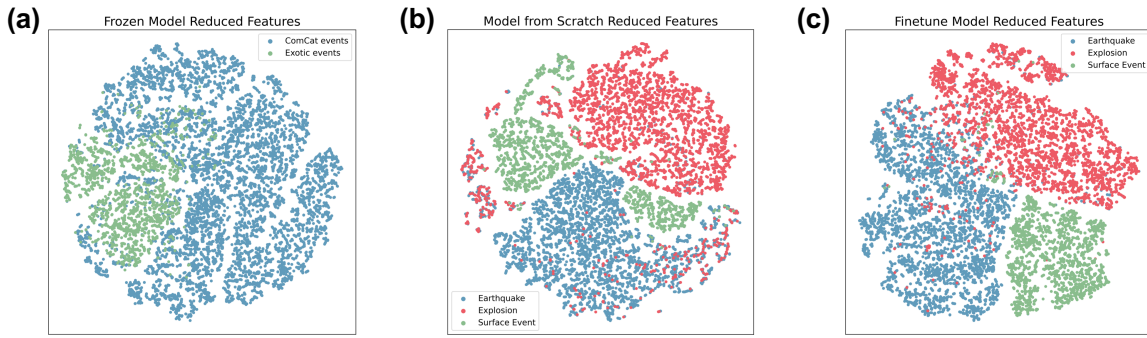


Figure S5: The visualization of reduced features of three models. (a - c) The reduced features from the frozen, scratch, and fine-tuned models, which is calculated through t-SNE. Given our model’s exclusive pre-training on earthquake events, the reduced features obtained from the frozen decoder are distinguishable primarily as ‘comcat events’ (including earthquake and explosions) or ‘exotic events’ (including surface events). Moreover, in the fine-tuned model, the reduced features associated with earthquakes, explosions, and surface events are distinctly separated from each other, showing a much clearer distinction compared to those in the scratch model.